RSC Advances

RSC Publishing

PAPER

View Article Online
View Journal | View Issue

Cite this: *RSC Advances*, 2013, **3**, 14007

Sequential covalent bonding activation and general base catalysis: insight into *N*-heterocyclic carbene catalyzed formylation of N–H bonds using carbon dioxide and silane†

Binju Wang and Zexing Cao*

The detailed catalytic mechanisms of *N*-heterocyclic carbenes (NHCs) in the formylation of N–H bonds using carbon dioxide and silane were investigated using density functional theory (DFT) calculations. Among all the examined reaction pathways, we found that the most favorable pathway involves collaboration between the covalent bonding activation and general base catalysis. The overall reaction can be divided into four stages, including silane activation through a covalent bonding mechanism, CO_2 insertion into the Si–H bond of silane to yield a key intermediate formoxysilane (FOS), the NHC-catalyzed coupling of amine and FOS through a general base mechanism, and C–O bond breaking through general base catalysis to obtain the final amide product. The carbamic acid anion (Me_2NCOO^-) is an inevitable intermediate from the side reactions, and its formation is almost barrier free. NHC can act as a base to abstract a proton from the nucleophiles (such as amines or alcohol), and facilitate C–N bond or C–O bond formation or cleavage, and such a general base mechanism is remarkably favorable over the covalent binding mechanism for C–N bond (or C–O) bond formation (or cleavage). The calculated thermodynamic properties are in good agreement with the available experimental findings.

Received 26th March 2013,
Accepted 17th May 2013

DOI: 10.1039/c3ra41464g

www.rsc.org/advances

1. Introduction

Carbon dioxide (CO_2) has attracted unprecedented attention in the past several decades due to its significant effects on climate change, and extensive efforts have been devoted to the exploration of CO_2 fixation and its catalytic transformations.[1–5] CO_2, being nontoxic, abundant, and an economical C_1-carbon source, can be converted into a series of industrial products and fine chemicals.[1] Due to the thermodynamic and kinetic stability of CO_2, the utilization of CO_2 as a chemical feedstock is limited to a few industrial processes, including the synthesis of urea and its derivatives.[1]

Recently, Cantat and co-workers[5] developed a novel metal-free organocatalytic scheme for the synthesis of formamide based on CO_2/amine/silane three-component systems. Using *N*-heterocyclic carbenes (NHCs) as catalysts and silanes as reductants, they synthesized a variety of formamides with high yields from amines and CO_2 at room temperature (eqn (1)). This strategy allows efficient recycling of CO_2 and polymethylhydrosiloxane (PMHS), two abundant and nontoxic chemical waste compounds, and it should be especially attractive for CO_2 transformation and amide synthesis.

(1)

N-Heterocyclic carbenes (NHCs), known as versatile nucleophilic organocatalysts, can catalyze a large number of organic reactions.[6–8] It is commonly accepted that the catalytic role of NHCs is based on the covalent binding activation of the substrates. In fact, NHC–substrate adducts are formed in the vast majority of NHC-catalyzed transformations.[10] Due to their strong σ-donating ability, NHCs can activate a substrate by a covalent binding interaction, and this mode of action in catalysis is prevalent in previous studies. Alternatively, NHC may act as a base to abstract a proton from amines of the nucleophiles, and facilitate C–N bond formation with the carbonyl compounds. However, this catalytic activation mode has rarely been studied theoretically. Based on the H-bonding interaction analysis, Grimme *et al.* proposed that NHCs may act as cooperative catalysts in acylations of alcohols in the presence of amines.[9] On the one hand NHCs catalyze the oxidation reaction by covalent binding interaction. On the other hand NHCs activate the nucleophile of the alcohol through a general base mechanism. However, the mechanistic

State Key Laboratory of Physical Chemistry of Solid Surfaces and Fujian Provincial Key Laboratory of Theoretical and Computational Chemistry, College of Chemistry and Chemical Engineering, Xiamen University, Xiamen 360015, China.
E-mail: zxcao@xmu.edu.cn; Fax: +86-592-2183047

† Electronic supplementary information (ESI) available: Full geometric and energetic results, IRC results, complete ref. 10, and total energies and Cartesian coordinates of all the structures. See DOI: 10.1039/c3ra41464g

details of this transformation have not been available up to now.

Here, extensive density functional calculations have been performed to explore the catalytic role of *N*-heterocyclic carbenes in the formylations of N–H bonds using carbon dioxide and silane. Mechanistic details of different reaction pathways, structures and relative energies of species involved in the reactions have been reported. Our calculations show that both the covalent binding mode and general base catalysis play an important role in the NHC-catalyzed formylation of N–H bonds, which opens an alternative avenue toward understanding the catalytic role of *N*-heterocyclic carbenes in various organic reactions and the design of novel organocatalytic systems for organic synthesis.

2. Computational details

All calculations were performed with the Gaussian 09 package.[10] Geometries of all transition states, reactants, and intermediates involved in the reactions were fully optimized at the B97-D/6-31G(d) level of theory. B97-D was selected for its excellent performance in the determination of interaction energies for large vdW systems.[11,12] For comparison, other density functionals, including B3LYP and M06-2X, are also considered. Harmonic frequency calculations have been carried out at the equilibrium geometries to confirm the first-order saddle points and local minima on the potential energy surfaces, and to estimate the zero-point energy (ZPE), the thermal and entropic corrections at 298.15 K and 1 atm. The correlations between the stable structures and transition states were verified by analysis of the corresponding imaginary frequency modes and by intrinsic reaction coordinate (IRC) calculations. In particular, the B3LYP/6-31G(d) approach was also considered for unsuccessful IRC calculations by B97-D/6-31G(d). The relative energies of the B97-D/6-31G(d)-optimized geometries were further refined by single-point calculations at the B97-D/6-311+G(d,p) level with inclusion of solvent effects. The bulk solvation effects of THF were simulated by using the SMD solvent model.[13] We also compared the equilibrium structures optimized at the 6-31G(d) and 6-311+G(d,p) basis set levels for selected species involved in the general base mechanism and the covalent binding mechanism, and both calculations predict almost the same structural parameters for transition-state structures (Fig. S22 in ESI†). Natural bond orbital (NBO) analyses[14] at the B97-D/6-311+G(d,p) level were performed to assign the atomic charges. For bimolecular association processes, frequency calculations with the ideal gas model generally overestimate the entropic contribution significantly. Therefore, a correction of -2.6 kcal mol^{-1} was made to calibrate the free energy change for bimolecular association processes based on the 'theory of free volume'.[15]

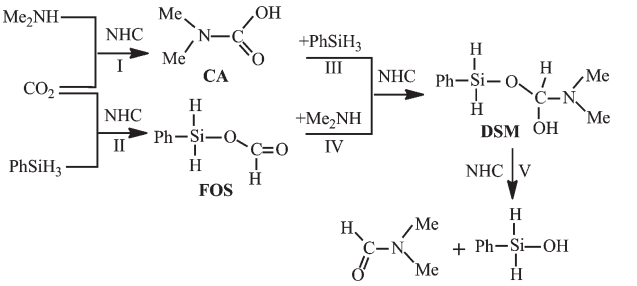

Scheme 1 Proposed mechanism for formylation of N–H bonds using carbon dioxide and silane.

3. Results and discussion

Here two possible reaction pathways have been envisioned for the overall transformation as depicted in Scheme 1. One is through the intermediate of the carbamic acid (**CA**), which is produced from the reaction of CO_2 and amine (stage I). The other is through the intermediate of formoxysilane (**FOS**), which is formed from the reaction of CO_2 and silane (stage II). Further reactions with the third substrate will afford the key intermediate (dimethylamino)(silyloxy)methanol (**DSM**). The final C–O bond cleavage, accompanied by deprotonation of the hydroxyl group, will yield the final amide product (stage V). Interestingly, both the covalent binding and general base mechanisms are available in stage I and stage IV (Scheme 2), as well as stage V. Take stage I as an example; NHCs may activate the substrate of CO_2 by a covalent binding interaction. Alternatively, NHCs may act as a base to abstract a proton from an amine, and facilitate C–N bond formation with CO_2. All these possible reaction mechanisms are explored and discussed in the following sections.

Stage I: CA formation

Fig. 1 presents the two possible reaction pathways for the formation of carbamic acid (**CA**), and the optimized structures

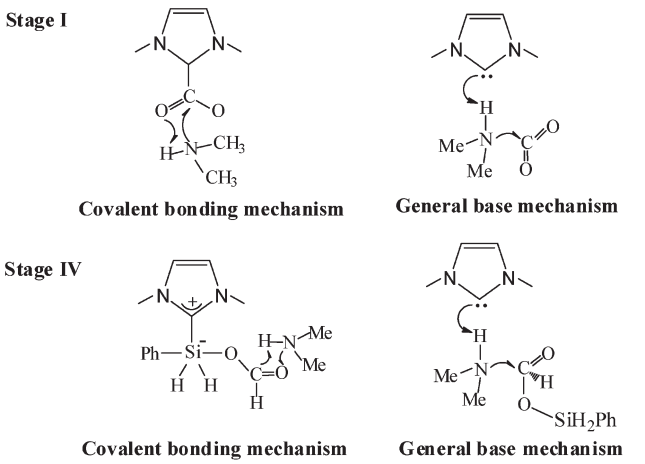

Scheme 2 Dual activation modes by NHCs: covalent binding mechanism and general base mechanism.

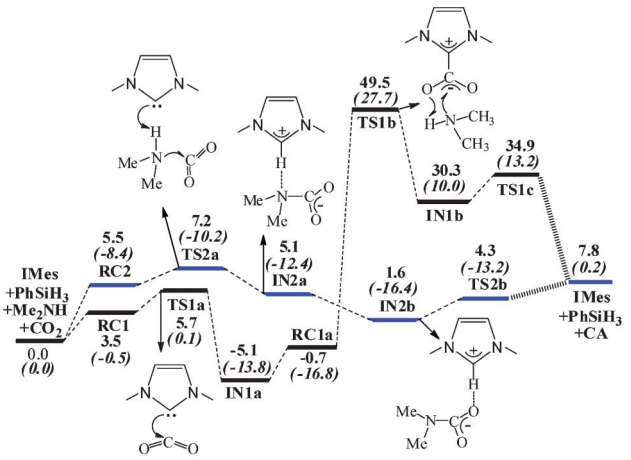

Fig. 1 Calculated relative energy profiles (in kcal mol^{-1}, the Gibbs energies are in normal font and the enthalpies are in italic font in parentheses) for **CA** formation in stage I at the B97-D/6-311+G(d,p)//6-31G(d) level.

of key species involved in the reaction are shown in Fig. 2. One pathway is through a covalent binding mechanism.

As shown in Fig. 1, CO_2 first approaches **IMes** and forms a reactant complex **RC1**. This process is endothermic by 3.5 kcal mol^{-1} in terms of the Gibbs energy. The electrophilic attack of CO_2 onto **IMes** *via* **TS1a** forms a Lewis acid–base adduct **IN1a**, with a free energy barrier of 5.7 kcal mol^{-1} relative to its initial components. **IN1a** is more stable than the initial complex **RC1** by 8.6 kcal mol^{-1}. **IN1a** has been isolated and fully characterized experimentally.[16] The following addition of Me_2NH onto the carbonyl group of **IN1a** *via* **TS1b** experiences a substantially high free energy barrier of 49.5 kcal mol^{-1}. Natural population analyses reveal that the negative charges on the CO_2 moiety increase to −0.607 e in the NHC–CO_2 adduct, and the positive charges on the C atom of the CO_2 moiety decrease to 0.693 e (0.948 e for free CO_2). This suggests that nucleophilic attack by amines on the carboxyl C atom will become more difficult. The final fragmentation of **IN1b** *via* **TS1c** leads to the formation of NHC and the carbamic acid (**CA**) intermediate. Overall, the formation of carbamic acid (**CA**) is endergonic by 7.8 kcal mol^{-1}.

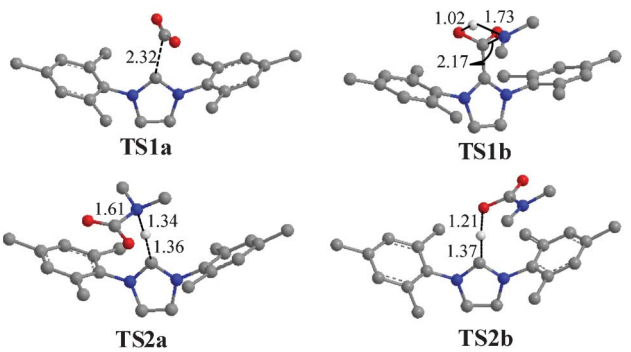

Fig. 2 Optimized structures (in Å) of key species involved in **CA** formation in stage I. For clarity, some unimportant H atoms are omitted.

The other route is through a general base mechanism. The reaction starts from a weak van der Waals complex (**RC2**), where Me_2NH forms a hydrogen bond with the carbene carbon. The electrophilic attack of the carbonyl carbon of CO_2 onto the N atom of Me_2NH (**TS2a**), coupled with the concerted proton abstraction by NHC, yields an intermediate **IN2a**. This step experiences an overall free energy barrier of only 7.2 kcal mol^{-1} relative to the isolated components. Here, the ''overall free energy barrier'' refers to the free energy barrier relative to the initial separated reactants, which is directly connected with the overall rate constant. In this process, NHC acts as a base to abstract the proton of Me_2NH nitrogen, and the deprotonation of the amino group significantly increases the negative charge of the amino N atom (−0.878 e in free Me_2N^- *vs.* −0.666 e in Me_2NH), so that the nucleophilicity of the Me_2NH nitrogen is significantly enhanced. The subsequent hydrogen abstraction from NHC by the newly-generated ^-O_2C–$N(Me)_2$ moiety through **TS2b** yields the **CA** intermediate.

The predicted free energy barrier for this step is only 2.7 kcal mol^{-1}. Clearly, inspection of the results in Fig. 1 (**TS1b** *vs.* **TS2a**) reveals that the general base mechanism (7.2 kcal mol^{-1}) is remarkably favorable over the covalent binding mechanism (49.5 kcal mol^{-1}). Due to their strong σ-donating ability, NHCs can either activate the substrate by a covalent binding interaction, or act as a base to abstract a proton from the nucleophile amines. In the covalent binding mechanism, the strong σ-donating ability of NHCs decreases the positive charge of the C atom in the CO_2 moiety, so that nucleophilic attack by amines on the carboxyl C atom becomes more difficult. This has been verified by the calculated barriers. The free energy barrier for the uncatalyzed pathway is 36.6 kcal mol^{-1} (see Fig. S4, ESI†), even lower than that of the covalent binding mechanism (49.5 kcal mol^{-1}). In the general base mechanism, the nucleophilicity of Me_2NH is substantially increased by deprotonation of the N–H group, and thus the C–N bond coupling becomes extremely facile. For comparison, we also considered the one additional amine catalyzed reaction of Me_2NH with CO_2 (see Fig. S5 in ESI†). The second amine catalyzed pathway experiences a free energy barrier of 13.0 kcal mol^{-1}, much higher than that of the general base mechanism, indicating that the NHC-catalyzed transformation is still the dominating pathway.

Stage II: FOS formation

Fig. 3 presents the two possible reaction pathways for **FOS** formation from the reactions of CO_2 and silane. These reactions have been systematically investigated at the M05-2X level by Wang and co-workers.[8a] As shown in Fig. 3, one pathway is CO_2 activation in the initial reaction, and the other is $PhSiH_3$ activation in the initial reaction. Both reactions proceed through the covalent binding mechanism. It was found that NHC can significantly activate the Si–H bond of silane by pushing more electron density to the H atoms, and thus CO_2 can easily insert into the Si–H bond of silane and form a formoxysilane (**FOS**) intermediate.[8a] For comparison, we also examined the possibility of a general base mechanism for **FOS** formation, in which attack of the negatively charged carbonyl O of CO_2 onto the positively charged Si atom of $PhSiH_3$ is coupled with concerted H abstraction (from the Si–H

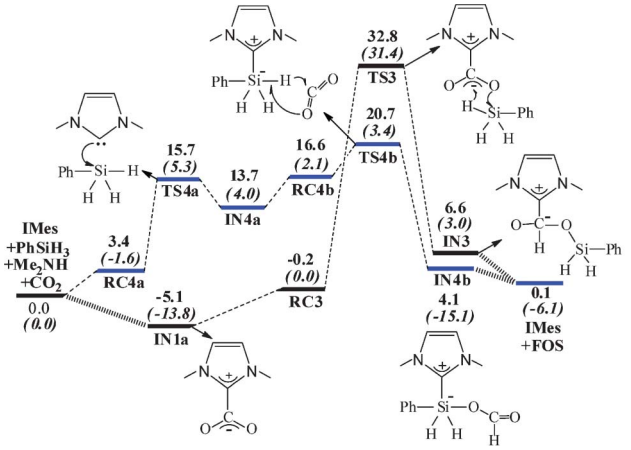

Fig. 3 Calculated relative energy profiles (in kcal mol^{-1}, the Gibbs energies are in normal font and the enthalpies are in italic font in parentheses) for **FOS** formation in stage II at the B97-D/6-311+G(d,p)//6-31G(d) level.

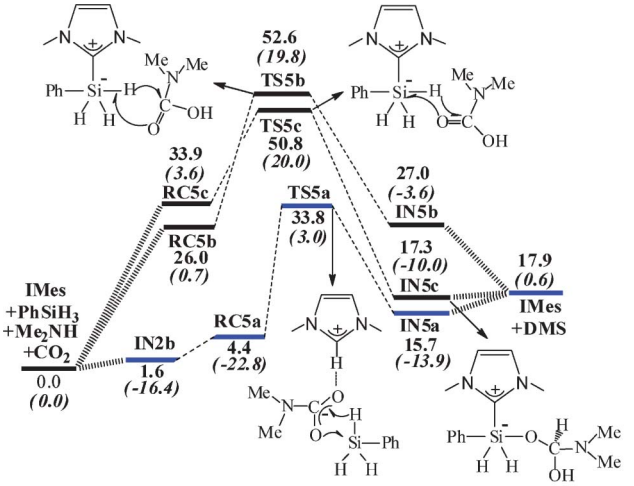

Fig. 4 Calculated relative energy profiles (in kcal mol^{-1}, the Gibbs energies are in normal font and the enthalpies are in italic font in parentheses) for **DSM** formation in stage III at the B97-D/6-311+G(d,p)//6-31G(d) level.

bond of $PhSiH_3$) by NHC. However, our calculations did not locate this transition state, because the Si–H bond of $PhSiH_3$ is different from the N–H bond (in amines) or O–H bond (in alcohols), and the H atom in $PhSiH_3$ is negatively charged (−0.147 e). Accordingly, here NHCs cannot act as a base to abstract a proton from the Si–H bond. The predicted free energy barriers at the M05-2X/6-311+G(d,p)//6-31G(d) level are 34.8 kcal mol^{-1} for the CO_2 activation pathway, and 30.6 kcal mol^{-1} for the $PhSiH_3$ activation pathway, respectively, from previous calculations.[8a] As Fig. 3 shows, the B97-D calculations here yield a free energy barrier of 32.8 kcal mol^{-1} for the CO_2 activation pathway, and 20.7 kcal mol^{-1} for the $PhSiH_3$ activation pathway relative to the initial reactants. Overall, the $PhSiH_3$ activation pathway is much favorable over the CO_2 activation pathway.

As shown in Table 1, the predicted free energy barriers and free energy changes in bimolecular association processes are quite sensitive to the choice of methodology. B3LYP predicts a substantially high free energy barrier of 51.2 kcal mol^{-1}. Moreover, the binding energies in bimolecular association processes are notably underestimated by B3LYP. Significantly improved results are obtained by using M06-2X, in which dispersion effects are taken into account. It can be expected that the Grimme's dispersion-corrected B97-D functional yields the most reliable structures and relative energies here, since B97-D can provide accurate binding energies for vdW systems.[11,12,17] Since the C–N coupling reaction step is also a significant step, we also tested **TS2a** by M06-2X and B3LYP. M06-2X predicts a free energy barrier of 7.2 kcal mol^{-1} (Fig. S23, ESI†), the same as the B97-D results (Fig. 1), but B3LYP predicts a free energy barrier of 20.4 kcal mol^{-1} (Fig. S24, ESI†), much higher than M06-2X and B97-D. Moreover, it seems difficult to explain these differences based on their optimized structures, since there are only quite small differences in geometries for different methods (see Fig. 2, Fig. S23, and Fig. S24, ESI†).

Table 1 Calculated thermodynamic values at 298 K (in kcal mol^{-1}) for **FOS** formation with different methods[a]

Method	ΔG_r		$\Delta G^{\neq}$
	IMes + $PhSiH_3$ → RC4a	IN4a + CO_2 → RC4b	
B3LYP[b]	12.8	8.8	51.2
M06-2X[c]	7.0	3.6	27.7
B97-D	3.4	2.9	20.7

[a] ΔG_r is the free energy change for the bimolecular association process; $\Delta G^{\neq}$ is the overall free energy barrier. [b] Optimized geometries by B3LYP/6-31G(d) and the single-point energy calculations by B3LYP/6-311+G(d,p). [c] Optimized geometries by M06-2X/6-31G(d) and the single-point energy calculations by M06-2X/6-311+G(d,p).

Stage III: DSM formation from the CA intermediate

Fig. 4 summarizes the three reaction pathways for **DSM** formation from the reactions of **CA** intermediate and $PhSiH_3$, and the optimized structures of key species involved in the reaction are shown in Fig. 5. The hydrosilylation of carbamate anion by $PhSiH_3$ through **TS5a** yields the intermediate **IN5a**. This pathway requires an overall free energy barrier of 33.8 kcal mol^{-1}. We note that here the proton from the NHC carbon finally migrates to the carbonyl oxygen of **DSM** in the reaction process as indicated from the IRC calculations (Fig. S15†). For the other two reaction pathways, the Si–H bond of silane is firstly activated by the covalent bonding interaction, and then the carbonyl group of **CA** inserted into the Si–H bond of silane. Two distinct transition-state structures **TS5b** and **TS5c** are identified in the present study. In **TS5b**, the positively charged carbonyl carbon (0.872 e) in **CA** firstly abstracts a negatively charged H atom (−0.298 e) from the silane, and then the carbonyl oxygen couples with the Si atom to form a new bond. In **TS5c**, the negatively charged carbonyl oxygen (−0.636 e) firstly attacks the positively charged Si of silane (0.854 e), and then the negatively charged H atom (−0.203 e) transfers to the carbonyl carbon. The calculated free energy

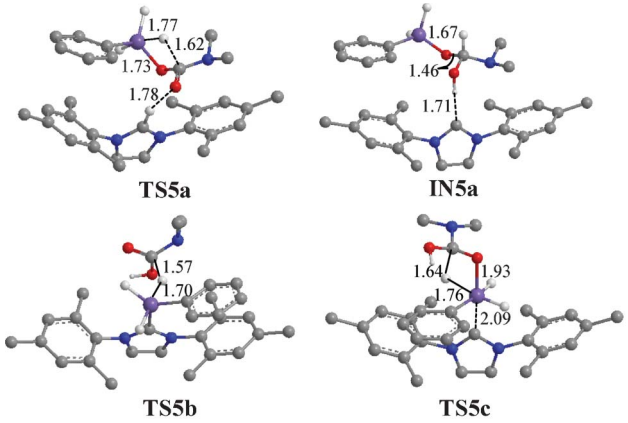

Fig. 5 Optimized structures (in Å) of key species involved in **DSM** formation in stage III. For clarity, some unimportant H atoms are omitted.

barriers are 52.6 kcal mol^{-1} in **TS5b** and 50.8 kcal mol^{-1} in **TS5c**, respectively. We note here that the barrier for CA insertion into the Si–H bond of silane (**TS5b**) is much higher than that of CO_2 insertion reaction in **TS4b** ($\Delta G^{\neq}$ = 20.7 kcal mol^{-1}). This may arise from two aspects. On the one hand, the positive charge of the carbonyl carbon in carbamic acid (0.885 e in **RC5b**) is lower than that in CO_2 (0.948 e). On the other hand, the center carbonyl carbon forms a rigid plane in the carbamic acid, which makes it relatively hard to twist.

Stage IV: DSM formation from the FOS intermediate

Next, we considered **DSM** formation from the reactions of the **FOS** intermediate and amine. Fig. 6 presents the two possible reaction pathways, and the optimized structures of key species involved in the reaction are shown in Fig. 7. One pathway is through the covalent binding mechanism *via* **TS6a**, in which the Si atom of **FOS** is covalently bonded to the NHC carbon, and then the C=O double bond undergoes a concerted addition by Me_2NH through **TS6a**. The predicted free energy barrier is 50.3 kcal mol^{-1}. Natural population analyses reveal

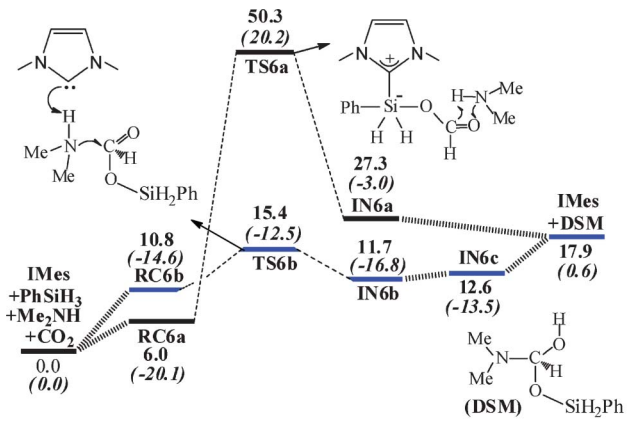

Fig. 6 Calculated relative energy profiles (in kcal mol^{-1}, the Gibbs energies are in normal font and the enthalpies are in italic font in parentheses) for **DSM** formation in stage IV at the B97-D/6-311+G(d,p)//6-31G(d) level.

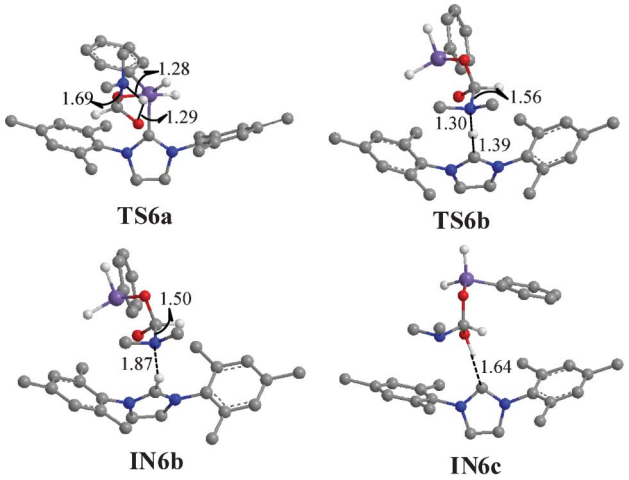

Fig. 7 Optimized structures (in Å) of key species involved in **DSM** formation in stage IV. For clarity, some unimportant H atoms are omitted.

that the positive charge of the carbonyl carbon atom in **RC6a** is reduced to 0.643 e, compared to 0.693 e in the NHC–CO_2 adduct (**IN1a**), and such a decrease of positive charge on the carbonyl carbon makes its electrophilic ability even weaker, resulting in an even higher barrier than that in **TS1b** ($\Delta G^{\neq}$ = 49.5 kcal mol^{-1}). The other pathway is the general base mechanism through **TS6b**. The reaction starts from a weak van der Waals complex (**RC6b**), where Me_2NH forms a hydrogen bond with the carbene carbon. The nucleophilic attack of the N atom of Me_2NH onto the carbonyl carbon of **FOS** *via* **TS6b**, coupled with the concerted proton abstraction by NHC, yields an intermediate **IN6b**. This step experiences a free energy barrier of 15.4 kcal mol^{-1}. Similarly as in **TS2a**, NHC acts as a base to abstract the proton of the Me_2NH nitrogen, and the deprotonation of the amino group significantly increases the negative charge on the amino N atom, so that the nucleophilicity of the Me_2NH nitrogen is significantly enhanced. Clearly, the general base mechanism (**TS6b**) is remarkably favorable over the covalent binding mechanism (**TS6a**). The subsequent proton transfer from the NHCs to the $^{-}$O–C moiety yields the **DSM** intermediate (**IN6c**). Comparison of the results in Fig. 3 and Fig. 5 reveals that **DSM** formation through the **FOS** intermediate is remarkably favorable over the pathway *via* the intermediate **CA**.

Stage V: amide formation

In this section, we consider amide formation from the **DSM** intermediate. Fig. 8 presents the two possible reaction pathways for generating the amide, and the optimized structures of key species involved in the reaction are shown in Fig. 9. These two reaction pathways correspond to the covalent binding mechanism and the general base mechanism, respectively. The covalent binding mechanism involves a cyclic transition state of **TS7a**, in which C–O bond cleavage is coupled with the formation of a H_2 molecule. This pathway experiences a free energy barrier of 32.9 kcal mol^{-1}. The other pathway is a general base mechanism. The reaction starts from the complex of **IN5a** (also shown in Fig. 4), where **DSM** forms a hydrogen

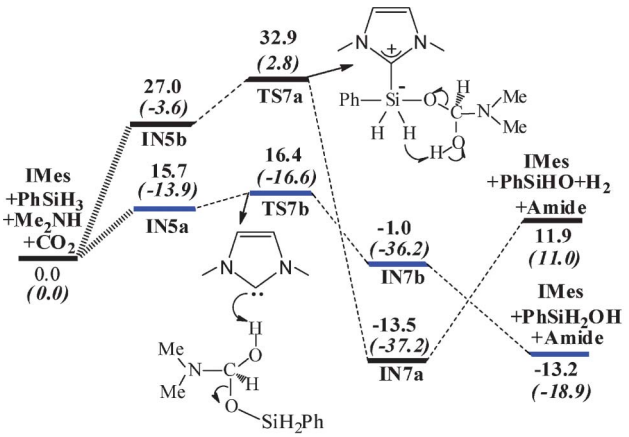

Fig. 8 Calculated relative energy profiles (in kcal mol^{-1}, the Gibbs energies are in normal font and the enthalpies are in italic font in parentheses) for amide formation from **DSM** in stage V at the B97-D/6-311+G(d,p)//6-31G(d) level.

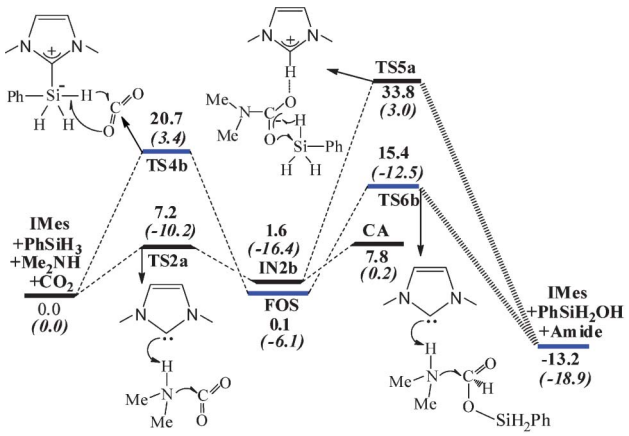

Fig. 10 Relative energy profiles (in kcal mol^{-1}, the Gibbs energies are in normal font and the enthalpies are in italic font in parentheses) of two general reaction pathways for amide formation.

bond with the carbene carbon. **IN5a** can undergo C–O bond dissociation through **TS7b**, leading to formation of the final product formamide. Interestingly, here NHC also acts as a base catalyst, and the ''concerted'' transition state **TS7b** shows a highly stepwise character, in which the hydroxyl H atom of the substrate is first abstracted by the NHC carbon atom, and then C–O bond cleavage leads to the formation of a $PhSiH_2O^-$ moiety, and the final proton transfer from the NHC carbon to the $PhSiH_2O^-$ moiety yields the complex **IN7b**. The predicted free energy barrier in this pathway is 16.4 kcal mol^{-1}. Overall, the general base mechanism is also remarkably favorable over the covalent binding mechanism.

Overall reaction mechanisms for amide formation

So far, the overall catalytic mechanisms are quite clear as displayed in Fig. 10. Two general reaction pathways lead to the formation of amide. One is through the intermediate of the carbamate anion (Me_2NCOO^-), while the other is through the intermediate of formoxysilane (**FOS**). The pathway *via* the intermediate of **FOS** experiences a free energy barrier of 20.7 kcal mol^{-1}, while the pathway *via* the intermediate of the carbamate anion (**IN2b**) requires an overall free energy barrier of 33.8 kcal mol^{-1}. Accordingly, the reaction pathway *via* the **FOS** intermediate is much more favorable than the pathway *via* the **CA** intermediate, so **FOS** is the real intermediate responsible for amide formation. **FOS** formation is the rate-determining step in the overall transformation. The predicted overall free energy barrier by B97-D is 20.7 kcal mol^{-1} in **IMes** catalyst. For comparison, we also examined the substrate of morpholine in **IPr** catalyst; the calculated free energy barrier is 18.6 kcal mol^{-1} (Fig. S21, ESI†), in good agreement with the experimental value of 19.0 kcal mol^{-1}.[18] Actually, the intermediate **FOS** was detected in NHC-catalyzed conversion of carbon dioxide into methanol,[3j] which bears quite similar reaction conditions to Cantat's experiment. Both the carbamate anion and **CA** are just intermediates from the side reactions, though their formations are quite facile. Moreover, both the carbamate anion and **CA** can also be converted into the final product amide through a series of reverse transformations as shown in Fig. 10, and these transformations are even more favorable thermodynamically than the initial substrates of amines and CO_2. These above results can explain why carbamic acid [Me_2NCO_2H] or the carbamate anion [Me_2NCOO^-] itself can be used as efficient substrates for amide formation.

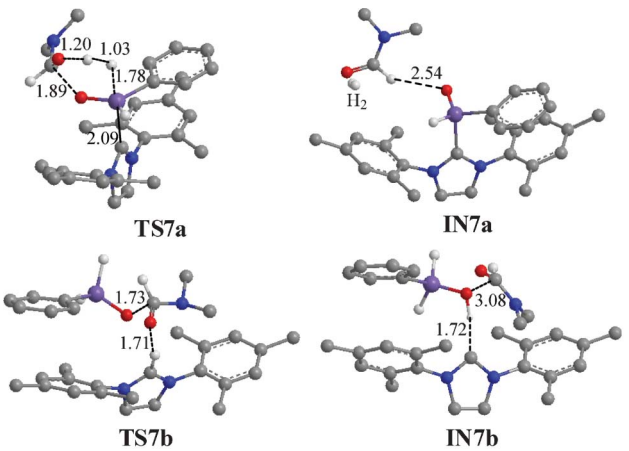

Fig. 9 Optimized structures (in Å) of key species involved in the amide formation from **DSM** in stage V. For clarity, some unimportant H atoms are omitted.

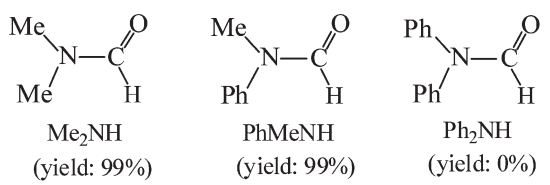

Scheme 3 Different amine substrates and their yields in Cantat *et al.*'s experiment.

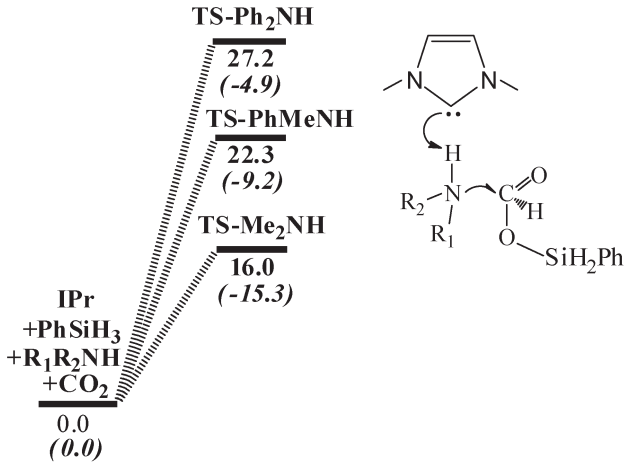

Fig. 11 Calculated relative energies of the transition state (in kcal mol^{-1}, the Gibbs energies are in normal font and the enthalpies are in italic font in parentheses) for C–N coupling reactions for different amines at the B97-D/6-311+G(d,p)//6-31G(d) level.

Phenyl substitution effects on the reactivity of the amines

Experimental investigations by Cantat and co-workers[5] revealed that the aromatic amine PhMeNH is also an active substrate, with conversion yields of up to 99% as shown in Scheme 3. However, two phenyl substitutions at the amine nitrogen completely shut down the reaction. According to the overall reaction mechanisms in Fig. 10, the substrate amine is only actively involved in stage IV of the C–N coupling reactions. Fig. 11 compares the relative energies of the transition state for C–N coupling reactions for different amines. Since **IPr** catalyst was used in the experiments, here the calculations are based on the **IPr** catalyst for consistency. For the unsubstituted amine Me_2NH, the predicted Gibbs energy barrier is 16.0 kcal mol^{-1}. For one phenyl substituted amine PhMeNH, the Gibbs energy barrier increases to 22.3 kcal mol^{-1}. When the second phenyl is introduced into amine (Ph_2NH), the Gibbs energy barrier further increases to 27.2 kcal mol^{-1}. These results are in good agreement with experimental findings that two phenyl substitutions at the amine nitrogen can completely shut down the reaction due to high barriers.[5]

Aromatic substituents on the nitrogen atoms of amines have remarkable effects on the activities of substrates. On the one hand, the electron-withdrawing character of the phenyl ring can reduce the basicity of an amine. In Me_2NH, the deprotonation of the amino group can significantly increase the negative charge of the amino N atom (−0.878 e in free Me_2N^- *vs.* −0.666 e in Me_2NH), and thus increase the nucleophilicity of the amine for C–N coupling. In the case of Ph_2NH, however, the negative charge at the N atom of the Ph_2N^- moiety does not increase significantly compared with its neutral counterpart (−0.619 e in free Ph_2N^- *vs.* −0.579 e in Ph_2NH), since the negative charges are well delocalized over the double phenyl rings, quite different from the case of Me_2NH. Therefore, the nucleophilicity of Ph_2NH is remarkably weakened by the double phenyl substitution. Overall, the negative charges on the N-atoms of Me_2N^-, $PhMeN^-$, and Ph_2N^- anions are −0.878 e, −0.673 e, and −0.619 e, respectively. The order of negative charges on the N atoms has excellent correlation with the calculated Gibbs energy barriers in the C–N coupling, which are 16.0 kcal mol^{-1} for Me_2NH, 22.3 kcal mol^{-1} for PhMeNH, and 27.2 kcal mol^{-1} for Ph_2NH, respectively. These results also show good agreement with the experiments both qualitatively and quantitatively. The high barrier of 27.2 kcal mol^{-1} for Ph_2NH can shut down this reaction at room temperature as observed in experiments, and thus diphenylamine is unreactive in the formylation reaction.

4. Conclusion

In the present work, we reported a comprehensive theoretical study on the catalytic mechanism of *N*-heterocyclic carbenes in the formylation of N–H bonds using carbon dioxide and silane. Among all the examined reaction pathways, we found that the most favorable pathway involves collaboration between covalent bonding activation and general base catalysis. The overall reaction can be divided into four steps, including silane activation through a covalent bonding mechanism, CO_2 insertion into the Si–H bond of silane to yield a key intermediate formoxysilane (**FOS**), NHC-catalyzed coupling of amine and **FOS** through a general base mechanism, and C–O bond breaking through a general base mechanism to obtain the final amide product. NHCs can act as a base to abstract a proton from the nucleophile (such as amines or alcohol), and facilitate C–N bond or C–O bond formation or cleavage. As shown in the present study, the general base mechanism is remarkably favorable over the covalent binding mechanism for the C–N bond coupling. The present mechanistic investigations provide a basis to further understand the catalytic role of *N*-heterocyclic carbenes as metal-free catalysts in various organic reactions, and assist us to develop new organocatalytic systems.

Acknowledgements

This work was supported by the Ministry of Science and Technology (2011CB808504 and 2012CB214900) and the National Science Foundation of China (21133007).

References

1 For recent reviews on CO_2 fixation and transformation, see:(*a*) T. Sakakura, J. C. Choi and H. Yasuda, *Chem. Rev.*, 2007, **107**, 2365; (*b*) G. Centi and S. Perathoner, *Catal. Today*, 2009, **148**, 191; (*c*) K. M. K. Yu, I. Curcic, J. Gabriel and S. C. E. Tsang, *ChemSusChem*, 2008, **1**, 893; (*d*) V. P. Indrakanti, J. D. Kubicki and H. H. Schobert, *Energy Environ. Sci.*, 2009, **2**, 745; (*e*) M. Mikkelsen, M. Jorgensen and F. C. Krebs, *Energy Environ. Sci.*, 2010, **3**, 43; (*f*) S. N. Riduan and Y. G. Zhang, *Dalton Trans.*, 2010, **39**, 3347; (*g*) K. Huang, C. L. Sun and Z. J. Shi, *Chem. Soc. Rev.*, 2011,

40, 2435; (*h*) M. Cokoja, C. Bruckmeier, B. Rieger, W. A. Herrmann and F. E. Kuehn, *Angew. Chem., Int. Ed.*, 2011, **50**, 8510; (*i*) M. R. Kember, A. Buchard and C. K. Williams, *Chem. Commun.*, 2011, **47**, 141; (*j*) W. Wang, S. Wang, X. Ma and J. Gong, *Chem. Soc. Rev.*, 2011, **40**, 3703; (*k*) D. J. Darensbourg, *Chem. Rev.*, 2007, **107**, 2388.

2 For selected recent papers on CO_2 fixation and transformation, see: (*a*) D. Huang, O. V. Makhlynets, L. L. Tan, S. C. Lee, E. V. Rabak-Akimova and R. H. Holm, *Proc. Natl. Acad. Sci. U. S. A.*, 2011, **108**, 1222; (*b*) R. Vaidhyanathan, S. S. Iremonger, G. K. H. Shimizu, P. G. Boyd, S. Alavi and T. K. Woo, *Science*, 2010, **330**, 650; (*c*) H. Zhou, W. Z. Zhang, Y. M. Wang, J. P. Qu and X. B. Lu, *Macromolecules*, 2009, **42**, 5419; (*d*) T. M. McDonald, D. M. D'Alessandro, R. Krishna and J. R. Long, *Chem. Sci.*, 2011, **2**, 2022; (*e*) C. M. Momming, E. Otten, G. Kehr, R. Frohlich, S. Grimme, D. W. Stephan and G. Erker, *Angew. Chem., Int. Ed.*, 2009, **48**, 6643; (*f*) R. Dawson, D. J. Adams and A. I. Cooper, *Chem. Sci.*, 2011, **2**, 1173; (*g*) L. Dostal, R. Jambor, A. Ruzicka, M. Erben, R. Jirasko, E. Cernoskova and J. Holecek, *Organometallics*, 2009, **28**, 2633; (*h*) U. Patil, A. Fihri, A. H. Emwas and V. Polshettiwar, *Chem. Sci.*, 2012, **3**, 2224.

3 For selected recent papers on CO_2 fixation and transformation, see: (*a*) C. Das Neves Gomes, O. Jacquet, C. Villiers, P. Thuery, M. Ephritikhine and T. Cantat, *Angew. Chem., Int. Ed.*, 2012, **51**, 187; (*b*) G. Menard and D. W. Stephan, *J. Am. Chem. Soc.*, 2010, **132**, 1796; (*c*) A. E. Ashley, A. L. Thompson and D. O'Hare, *Angew. Chem., Int. Ed.*, 2009, **48**, 9839; (*d*) A. Berkefeld, W. E. Piers and M. Parvez, *J. Am. Chem. Soc.*, 2010, **132**, 10660; (*e*) G. Menard and D. W. Stephan, *Angew. Chem., Int. Ed.*, 2011, **50**, 8396; (*f*) D. J. Darensbourg, *Inorg. Chem.*, 2010, **49**, 10765; (*g*) S. Chakraborty, J. Zhang, J. A. Krause and H. Guan, *J. Am. Chem. Soc.*, 2010, **132**, 8872; (*h*) D. P. Hruszkewycz, J. Wu, N. Hazari and C. D. Incarvito, *J. Am. Chem. Soc.*, 2011, **133**, 3280; (*i*) C. A. Huff and M. S. Sanford, *J. Am. Chem. Soc.*, 2011, **133**, 18122; (*j*) S. N. Riduan, Y. G. Zhang and J. Y. Ying, *Angew. Chem., Int. Ed.*, 2009, **48**, 3322; (*k*) Y. G. Zhang and S. N. Riduan, *Angew. Chem., Int. Ed.*, 2011, **50**, 6210; (*l*) E. Balaraman, C. Gunanathan, J. Zhang, L. J. W. Shimon and D. Milstein, *Nat. Chem.*, 2011, **3**, 609.

4 For some theoretical studies of CO_2 fixation and transformation, see: (*a*) Y. Y. Ohnishi, T. Matsunaga, Y. Nakao, H. Sato and S. Sakaki, *J. Am. Chem. Soc.*, 2005, **127**, 4021; (*b*) F. Huang, C. Zhang, J. Jiang, Z. X. Wang and H. Guan, *Inorg. Chem.*, 2011, **50**, 3816; (*c*) T. J. Schmeier, G. E. Dobereiner, R. H. Crabtree and N. Hazari, *J. Am. Chem. Soc.*, 2011, **133**, 9274; (*d*) R. Tanaka, M. Yamashita, L. W. Chung, K. Morokuma and K. Nozaki, *Organometallics*, 2011, **30**, 6742; (*e*) A. Uhe, M. Hölscher and W. Leitner, *Chem.–Eur. J.*, 2012, **18**, 170; (*f*) M. J. Ajitha and C. H. Suresh, *J. Org. Chem.*, 2012, **77**, 1087; (*g*) L. Dang, Z. Lin and T. B. Marder, *Organometallics*, 2010, **29**, 917; (*h*) M. Wang, T. Fan and Z. Lin, *Organometallics*, 2012, **31**, 560.

5 O. Jacquet, C. Das Neves Gomes, M. Ephritikhine and T. Cantat, *J. Am. Chem. Soc.*, 2012, **134**, 2934.

6 For some recent reviews of NHC organocatalysts, see: (*a*) D. Enders, O. Niemeier and A. Henseler, *Chem. Rev.*, 2007, **107**, 5606; (*b*) N. Marion, S. Díes-González and S. P. Nolan, *Angew. Chem., Int. Ed.*, 2007, **46**, 2988; (*c*) P. Hoyos, J. Sinisterra, F. Molinari, A. R. Alcántara and P. D. María, *Acc. Chem. Res.*, 2010, **43**, 288; (*d*) A. T. Biju, N. Kuhl and F. Glorius, *Acc. Chem. Res.*, 2011, **44**, 1182; (*e*) V. Nair, R. S. Menon, A. T. Biju, C. R. Sinu, R. R. Paul, A. Jose and V. Sreekumar, *Chem. Soc. Rev.*, 2011, **40**, 5336; (*f*) A. Grossmann and D. Enders, *Angew. Chem., Int. Ed.*, 2012, **51**, 314; (*g*) X. Bugaut and F. Glorius, *Chem. Soc. Rev.*, 2012, **41**, 3511.

7 For some recent papers on NHC organocatalysts, see: (*a*) J. Kaeobamrung, J. Mahatthananchai, P. Zheng and J. W. Bode, *J. Am. Chem. Soc.*, 2010, **132**, 8810; (*b*) J. Mahatthananchai and J. W. Bode, *Chem. Sci.*, 2012, **3**, 192; (*c*) A. T. Biju, N. E. Wurz and F. Glorius, *J. Am. Chem. Soc.*, 2010, **132**, 5970; (*d*) E. M. Phillips, M. Riedrich and K. A. Scheidt, *J. Am. Chem. Soc.*, 2010, **132**, 13179; (*e*) R. L. Atienza, H. S. Roth and K. A. Scheidt, *Chem. Sci.*, 2011, **2**, 1772; (*f*) D. E. A. Raup, B. Cardinal-David, D. Holte and K. A. Scheidt, *Nat. Chem.*, 2010, **2**, 766; (*g*) X. Zhao, D. A. DiRocco and T. Rovis, *J. Am. Chem. Soc.*, 2011, **133**, 12466; (*h*) S. DeSarkar and A. Studer, *Angew. Chem., Int. Ed.*, 2010, **49**, 9266; (*i*) H. U. Vora and T. Rovis, *J. Am. Chem. Soc.*, 2010, **132**, 2860; (*j*) D. Cohen, B. Cardinal-David and K. A. Scheidt, *Angew. Chem., Int. Ed.*, 2011, **50**, 1678; (*k*) X. Bugaut, F. Liu and F. Glorius, *J. Am. Chem. Soc.*, 2011, **133**, 8130; (*l*) D. E. Cohen and K. A. Scheidt, *Chem. Sci.*, 2012, **3**, 53; (*m*) D. A. DiRocco and T. Rovis, *J. Am. Chem. Soc.*, 2011, **133**, 10402; (*n*) D. T. Cohen and K. A. Scheidt, *Chem. Sci.*, 2012, **3**, 53; (*o*) L. Candish and D. W. Lupton, *Chem. Sci.*, 2012, **3**, 380.

8 For some theoretical studies on NHC organocatalysts, see: (*a*) F. Huang, G. Lu, L. L. Zhao, H. X. Li and Z. X. Wang, *J. Am. Chem. Soc.*, 2010, **132**, 12388; (*b*) P. M. Zimmerman, A. Paul, Z. Y. Zhang and C. B. Musgrave, *Angew. Chem., Int. Ed.*, 2009, **48**, 2201; (*c*) L. Zhao, X. Y. Chen, S. Ye and Z. X. Wang, *J. Org. Chem.*, 2011, **76**, 2733; (*d*) P. Verma, P. A. Patni and R. B. Sunoj, *J. Org. Chem.*, 2011, **76**, 5606; (*e*) S. J. Ryan, A. Stasch, M. N. Paddon-Row and D. W. Lupton, *J. Org. Chem.*, 2012, **77**, 1113.

9 S. D. Sarkar, S. Grimme and A. Studer, *J. Am. Chem. Soc.*, 2010, **132**, 1190.

10 M. J. Frisch, *et al.*, *Gaussian 09, Revision B.01*, Gaussian, Inc., Wallingford, CT, 2009.

11 S. Grimme, *J. Comput. Chem.*, 2006, **27**, 1787.

12 (*a*) S. Grimme, J. Antony, T. Schwabe and C. MPck-Lichtenfeld, *Org. Biomol. Chem.*, 2007, **5**, 741; (*b*) J. Antony and S. Grimme, *Phys. Chem. Chem. Phys.*, 2006, **8**, 5287; (*c*) S. Grimme, *Angew. Chem., Int. Ed.*, 2008, **47**, 3430.

13 A. V. Marenich, C. J. Cramer and D. G. Truhlar, *J. Phys. Chem. B*, 2009, **113**, 6378.

14 (*a*) A. E. Reed and F. Weinhold, *J. Chem. Phys.*, 1983, **78**, 4066; (*b*) J. P. Foster and F. Weinhold, *J. Am. Chem. Soc.*, 1980, **102**, 7211.

15 (*a*) Q. Liu, Y. Lan, J. Liu, G. Li, Y.-D. Wu and A. Lei, *J. Am. Chem. Soc.*, 2009, **131**, 10201; (*b*) F. Schoenebeck and K. N. Houk, *J. Am. Chem. Soc.*, 2010, **132**, 2496; (*c*) A. Ariafard, N. J. Brookes, R. Stranger and B. F. Yates, *Organometallics*, 2011, **30**, 1340; (*d*) B. Liu, M. Gao, L. Dang, H. Zhao, T. B. Marder and Z. Lin, *Organometallics*, 2012, **31**, 3410; (*e*) S. W. Benson, *The Foundations of Chemical Kinetics*, R. E. Krieger, Malabar, FL, 1982.

16 H. A. Duong, T. N. Tekavec, A. M. Arif and J. Louie, *Chem. Commun.*, 2004, 112.

17 (*a*) R. A. Moss, L. Wang, C. M. Odorisio and K. Krogh-Jespersen, *J. Am. Chem. Soc.*, 2010, **132**, 10677; (*b*) L. Wang, R. A. Moss, J. Thompson and K. Krogh-Jespersen, *Org. Lett.*, 2011, **13**, 1198; (*c*) L. Wang, R. A. Moss and K. Krogh-Jespersen, *J. Phys. Chem. A*, 2011, **115**, 8113; (*d*) N. Sieffert and M. Bühl, *Inorg. Chem.*, 2009, **48**, 4622.

18 The experimental values of $\Delta G^{\neq}$ are derived from transition-state theory according to the experimental turnover frequency (TOF) and temperature (20 °C). For the substrate of morpholine in IPr catalyst, TOF = 160 h^{-1} at 20 °C, the estimated experimental $\Delta G^{\neq}$ is 19.0 kcal mol^{-1}.